

Flexible Magnetoreceptor with Tunable Intrinsic Logic for On-Skin Touchless Human-Machine Interfaces

Pavlo Makushko, Eduardo Sergio Oliveros Mata, Gilbert Santiago Cañón Bermúdez, Mariam Hassan, Sara Laureti, Christian Rinaldi, Federico Fagiani, Gianni Barucca, Nataliia Schmidt, Yevhen Zabala, Tobias Kosub, Rico Illing, Oleksii Volkov, Igor Vladymyrskyi, Jürgen Fassbender, Manfred Albrecht, Gaspare Varvaro,* and Denys Makarov*

Artificial magnetoception is a new and yet to be explored path for humans to interact with the surroundings. This technology is enabled by thin film magnetic field sensors embedded in a soft and flexible format to constitute magneto-sensitive electronic skins (e-skins). Being limited by the sensitivity to in-plane magnetic fields, magnetosensitive e-skins are restricted to basic proximity and angle sensing and are not used as switches or logic elements of interactive wearable electronics. Here, a novel magnetoreceptive platform for on-skin touchless interactive electronics based on flexible spin valve switches with sensitivity to out-of-plane magnetic fields is demonstrated. The technology relies on all-metal Co/Pd-based spin valves with a synthetic antiferromagnet possessing perpendicular magnetic anisotropy. The flexible magnetoreceptors act as logic elements, namely momentary and permanent (latching) switches. The switches maintain their performance even upon bending to a radius of less than 3.5 mm and withstand repetitive bending for hundreds of cycles. Here, flexible switches are integrated in on-skin interactive electronics and their performance as touchless human-machine interfaces is demonstrated, which are intuitive to use, energy efficient, and insensitive to external magnetic disturbances. This technology offers qualitatively new functionalities for electronic skins and paves the way towards full-fledged on-skin touchless interactive electronics.

1. Introduction

Flexible electronics is a game changer for prospective personal appliances and human-machine interfaces.^[1–4] There are already numerous demonstrations of mechanically imperceptible, wearable, and even on-skin interactive systems exploiting tactile,^[5–8] optical,^[9] electrical,^[10–12] and magnetic^[13–16] stimuli. Mechanically compliant magnetoresistive sensors were used as touchless human-machine interfaces enabling the interaction with magnetic objects by means of proximity sensing, motion, and orientation tracking features.^[13,15,17,18] Although basic interactive functionality has been demonstrated, the current on-skin magnetoreceptors are not employed as advanced spintronics-enabled switches and logic elements for skin compliant electronics. The major limitation remains on the material science side, primarily due to the use of

P. Makushko, E. S. Oliveros Mata, Dr. G. S. Cañón Bermúdez, Dr. Y. Zabala, Dr. T. Kosub, Dr. R. Illing, Dr. O. Volkov, Prof. J. Fassbender, Dr. D. Makarov

Helmholtz-Zentrum Dresden-Rossendorf e.V.
Institute of Ion Beam Physics and Materials Research
Dresden, Germany
E-mail: d.makarov@hzdr.de

P. Makushko, Dr. I. Vladymyrskyi
Paton Institute of Material Science and Electric Welding
National Technical University of Ukraine “Igor Sikorsky Kyiv Polytechnic Institute”

Prospect Peremogy 37, Kyiv 03056, Ukraine


M. Hassan, Dr. S. Laureti, Dr. G. Varvaro
Consiglio Nazionale delle Ricerche
Istituto di Struttura della Materia
nM2-Lab, Via Salaria km 29, 300 Monterotondo Scalo, Roma 00015, Italy
E-mail: gaspare.varvaro@ism.cnr.it

M. Hassan, Prof. G. Barucca
Università Politecnica delle Marche
Dipartimento SIMAU
Via Breccie Bianche 12, Ancona 60131, Italy

Prof. C. Rinaldi, Dr. F. Fagiani
Department of Physics
Politecnico di Milano
c/o via G. Colombo 81, Milano 20133, Italy

Dr. N. Schmidt, Prof. M. Albrecht
Institute of Physics
University of Augsburg
Universitätsstraße 1 Nord, D-86159 Augsburg, Germany

Dr. Y. Zabala
The H. Niewodniczanski Institute of Nuclear Physics
Polish Academy of Sciences
Krakow 31-342, Poland

 The ORCID identification number(s) for the author(s) of this article can be found under <https://doi.org/10.1002/adfm.202101089>.

© 2021 The Authors. Advanced Functional Materials published by Wiley-VCH GmbH. This is an open access article under the terms of the Creative Commons Attribution License, which permits use, distribution and reproduction in any medium, provided the original work is properly cited.

DOI: 10.1002/adfm.202101089

magnetic layer stacks, which are in-plane magnetized and, hence, are mainly sensitive to magnetic fields oriented in the sensor plane.^[13,15,16,19–35] The use of proximity sensors with in-plane sensitivity encumbers the readout of touchless on-skin switches, as magnetic objects approaching from directions other than the out-of-plane axis can falsely trigger switching. Introducing flexible Hall effect sensors^[36–39] could provide a solution to this conundrum, however, they cannot be intrinsically tuned to be bistable as needed for switches, and thus require additional flexible electronic modules. Considering the lower performance of flexible electronics compared to their rigid counterparts in terms of integration density and speed,^[16,40,41] full-fledged interactive systems should be built based on smart sensors with intrinsic logic functionality, which can be tailored by the material properties rather than by the circuit design.

In rigid electronics, including hard disk drives and magnetic random access memory elements, magnetic switches are typically built on spin valve (SV) layer stacks with out-of-plane easy axis of magnetization.^[42] The switching between two logical states “1” and “0” is uniquely encoded in the orientation of magnetization being pointing either up or down. This lifts any ambiguity in the interpretation of the logic state of the switch and makes SV switches an indispensable component of any spintronic circuit. These advanced sensing elements are substantially more demanding in the accuracy of the layer thickness and the interface quality. By now, reports are focused on the realization of flexible spin valve sensors with in-plane sensitivity only.^[33,43–45] The demonstration of mechanically flexible SVs with out-of-plane easy axis remains a major material science challenge in the community of flexible magnetoelectronics.

Here, we realize the first mechanically flexible SV switch sensitive to out-of-plane magnetic fields. The device consists of a Co/Pd-based spin valve stack with a synthetic antiferromagnetic reference layer possessing perpendicular magnetic anisotropy deposited onto a flexible polyethylene naphthalate (PEN) foil. By tuning the magnetic coupling in the SV layer stack via the choice of the thickness of the Cu spacer layer, we can tailor the flexible device to act as a momentary as well as permanent (latching) switch. The magnetoresistive performance of the SV switches does not degrade upon mechanical bending up to 3.5 mm. Furthermore, the devices withstand more than 600 bending cycles without sacrificing their performance. We demonstrate the advantages of the tunable logic functionality offered by our flexible SV switches by integrating them in an on-skin interactive system. The latching switches enable the realization of magnetic interfaces to permanently switch ON/OFF an electronic circuit in a touchless way. Due to the intrinsic memory function, the magnetic latching switches can reliably operate in an environment with strong magnetic disturbances. Momentary switches respond exclusively to one polarity of the magnetic field and can be used to temporarily switch on a virtual display when the SV switch is in proximity to a magnetic ON button. This operation mode is very useful for energy saving while interacting with displays, which is highly relevant for portable and wearable electronics. In this respect, the developed technology platform offers qualitatively new functionalities for on-skin touchless interactive systems, namely dedicated out-of-plane sensitivity and high tunability of the logic characteristics.

2. Results and Discussions

2.1. Flexible Magnetoreceptors

To realize flexible spin valves sensitive to out-of-plane magnetic fields, we deposited a layer stack consisting of a compensated synthetic antiferromagnet (SAF) $[\text{Co}(0.4)/\text{Pd}(0.9)]_4/\text{Ru}(0.4)/[\text{Co}(0.4)/\text{Pd}(0.9)]_3/\text{Co}(0.4)$ and a magnetic sensing layer $[\text{Co}(0.4)/\text{Pd}(0.9)]_2$ (numbers in brackets are thicknesses in nm) on PEN flexible foils with a thickness of 125 μm (Figure 1a). The thickness of the Cu spacer layer between the SAF and the magnetic sensing layer was changed between 2 and 5 nm to tailor the strength of the coupling between the two magnetic layers. Cross sectional transmission electron microscopy (TEM) images of the layer stack deposited on a PEN foil reveal firm adhesion of the metal layer stack to the foil and sharp interfaces in the SV stack (Figure 1b and Figure S1, Supporting Information) as needed for high magnetoresistive performance. A photograph of the flexible SV on a polymeric foil is shown in Figure 1c. Due to the thinness of the layer stack (about 30 nm), the samples are partly transparent (Figure S2, Supporting Information). Even when deposited on a PEN foil, the flexible SV switches maintain the magnetic properties of their rigid counterparts prepared on reference Si/SiO_x wafers (compare Figures S3 and S4, Supporting Information, for samples with different Cu spacer thickness). A typical three-step magnetization reversal behavior of the spin valve is observed in the magnetic hysteresis loops (Figure 1d,e (top panels) and Figure S5, Supporting Information). The corresponding magnetoresistive curves in Figure 1d,e (bottom panels) illustrate a sharp resistance switching as the magnetization of the magnetic sensing layer is reversed. The magnetoresistive (MR) ratio is defined as $MR = (R_{\uparrow\downarrow} - R_{\uparrow\uparrow}) / R_{\uparrow\uparrow}$ where $R_{\uparrow\downarrow}$ and $R_{\uparrow\uparrow}$ are the values of the electrical resistance corresponding to the antiparallel and parallel alignment of the magnetization of the ferromagnetic layers at the top and bottom interfaces of the Cu spacer layer. An MR ratio of about 2.5% is obtained for the samples with a Cu spacer thickness of 2 and 3 nm prepared on flexible PEN foils.

The switching fields of the sensing layer define the operation mode of the SV switch (momentary or latching). Tailoring the thickness of the Cu spacer layer allows adjusting the switching fields of the sensing layer in a wide range. We note that a qualitative change in the behavior of the SV is observed when the thickness of the Cu spacer layer changed from 2 to 3 nm (Figures S3 and S5, Supporting Information). Further increase in the Cu spacer thickness does not change the qualitative behavior of the SVs, but slightly decreases the magnitude of the MR effect due to the enhanced current shunting and scattering effects with the increase of Cu spacer layer thickness.^[46] The SV switch with a 2 nm thick Cu spacer layer reveals a shifted minor loop with both switching fields of the ascending and descending branches of the magnetoresistive curves positioned in the range of negative fields (Figure 1f, red line). In this case, the magnetoresistive switching can be actuated only by the application of a magnetic field oriented opposite to the magnetization of the SAF reference layer. This SV operates as a momentary switch, which responds to a magnetic field of a certain direction and will not be affected by a field of opposite polarity.

Increasing the Cu spacer thickness to 3 nm reduces the strength of the magnetic bias in the stack associated to

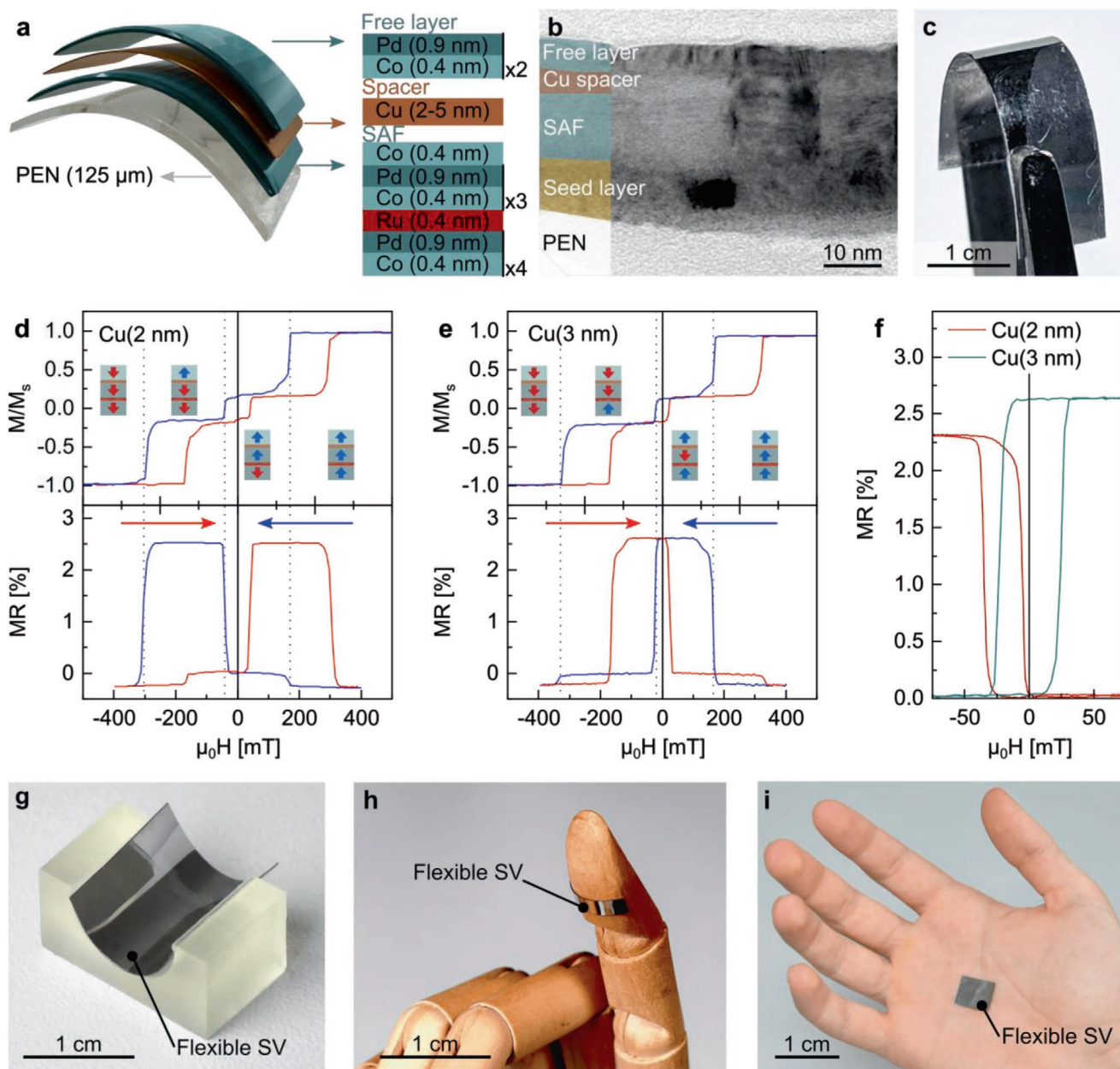


Figure 1. Flexible spin valves with out-of-plane sensitivity. a) Schematic representation of the Co/Pd-based spin valve stack. b) Cross-sectional TEM image of the spin valve deposited on a PEN flexible substrate. c) Optical micrograph of a flexible SV switch. Magnetic hysteresis loops (top panels) and corresponding magnetoresistive curves (bottom panels) measured of SV switches with a Cu spacer layer thickness of d) 2 and e) 3 nm. Magnetic field was applied perpendicular to the sample plane. Arrows indicate the direction of the magnetic field sweeping for ascending (red) and descending (blue) branches of the measured curves. Inset schematics in panels (d) and (e) represent a 3-step magnetization reversal process corresponding to blue branch of the hysteresis loops (further details are provided in Figure S5, Supporting Information). f) Magnetoresistive (MR) performance of the SV switches measured in a limited magnetic field range up to 150 mT after saturation of SAF in a positive field of +0.5 T. The samples with 2-nm and 3-nm-thick Cu spacer layer act as momentary and latching switches, respectively. Mechanical flexibility allows the spin valves to be integrated in g) processing tools, h) robotics, and i) on-skin interactive systems.

the magnetic coupling between the SAF reference layer and the free layer. The magnetoresistance curves become symmetric with respect to zero field. In this case, the initially programmed resistance state of the device is retained even after the magnetic field is removed. This SV operates as a latching switch, a key element of electronic circuits, typically used to maintain a state with lower current consumption and circuit complexity

compared to momentary switches. These elements are especially needed for flexible electronics to minimize the number of active elements for sensor conditioning. One of the major advantages given by the magnetic latching switch is that it becomes insensitive to magnetic disturbances, provided they do not exceed the switching field of the SV. Our samples are designed to have their switching fields in the range of 20 mT, which is substantially

larger than regular magnetic disturbances stemming from, e.g. power lines, electric transport, wireless communication systems.

We note that the latching functionality of the SV switch remains unchanged even when the sample is exposed to a magnetic field oriented under an angle to the easy axis (out-of-plane). The width of the magnetoresistive hysteresis of the magnetic sensing layer (minor loop) favorably increases up to about 40 mT when the magnetic field is applied at 80° with respect to the sample normal (Figures S6 and S7, Supporting Information). This makes the switch even more resilient against magnetic disturbances under realistic settings when the device is exposed to complex three-dimensional magnetic fields.

Due to their mechanical flexibility, these SV switches can find applications in various fields where conformal coating of a curved surface is needed, e.g. for processing tools (Figure 1g), robotics (Figure 1h), and on-skin electronics (Figure 1i).

2.2. Mechanical Performance of Flexible SV Switches

To assess their mechanical performance, the flexible SV switches were bent by moving two ends of the foil closer together from their initial flat state until a maximum bending radius of 3.5 mm was reached. Representative photographs showing a side view of the sample in a bent state are shown in Figure 2a. The photograph is color coded with respect to the change of the curvature radius along the sample. The corresponding strain in the metal stack for different curvature radii is shown in Figure 2b (see also Figure S8, Supporting Information). Scanning electron microscopy (SEM) images of the sample bent to 4 mm radius reveal no appearance of cracks or delamination (Figure 2c). The metal stack remains firmly attached to the polymeric foil. At a bending radius of 4 mm, the metal layer stack experiences a tensile strain of about 1.5%. When the sample is further bent to a 3.5 mm radius, the metal layer fractures (Figure 2d).

The MR ratio was measured in the bent state and after flattening the sample (Figure 2e). The MR ratio remains constant at the level of 2.5% independent of the bending radius. At the same time, the electrical resistance of the sample slightly increases in the bent state but fully recovers when the SV is flattened (Figure 2f). At the critical bending radius of 3.5 mm the electrical resistance of the SV sharply increases and is not fully recovered to its initial value upon flattening (Figure 2f, shaded region). However, functionality of the device is not affected and the MR ratio remains on the same level even when the sample is bent to 3.5 mm (Figure 2e). The increase of the sample resistance when approaching a 3.5 mm bending radius is caused by the appearance of a periodic fracture pattern in the metal films (Figure 2d and Figure S9, Supporting Information). Still, after the sample is flattened, the cracks close, which leads to the partial recovery of the sample resistance.

The impact of the cyclic bending on the MR performance of the SV switches was investigated by repeatedly bending the sample between radii of 28 mm and 14 mm for more than 600 cycles. The electrical resistance of the sample was continuously monitored revealing the stable device operation with a resistance change of 0.8% only (Figure 2g). Even after 600 bending cycles, the 2.5% MR effect remains and does not change compared to the flat samples.

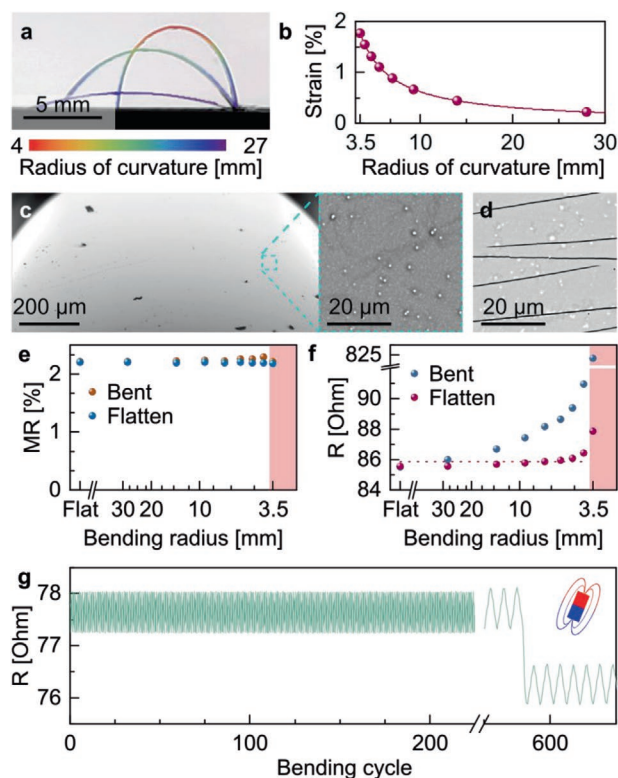


Figure 2. Mechanical and magnetoresistive performance of flexible spin valves upon bending. a) Optical photographs showing the sample at different bending radii. The photographs are color coded with the distribution of the radius of curvature along the SV. b) Tensile strain in the metal film as a function of radius of curvature. c) Overview SEM micrograph of the bent surface of the spin valve. The sample is bent to a radius of 4 mm. Inset shows a top view SEM micrograph focused on the most curved region of the sample. d) SEM micrograph of the fracture pattern on the sample bent to a radius of 3.5 mm. e) MR ratio and f) electrical resistance measured of the SV switch bent to the indicated radius. The measurement was carried out in the bent state (red symbols) and after the sample was flattened out (blue symbols). g) Cyclic bending test showing the change of the electrical resistance of the SV during more than 600 bending cycles between radii 28 and 14 mm. The zoom around the 600th bending cycle indicates the change of the SV resistance when the device is exposed to the field of a permanent magnet with a strength of about 100 mT at the device location.

2.3. Interactive Smart Skin Demonstration

We explore the application potential of these SV switches with different thickness of the Cu spacer layer as functional elements of interactive on-skin electronics. In contrast to regular proximity sensors based on giant magnetoresistive (GMR) multilayers (Figure S10, Supporting Information), SV switches act as logic elements of the electronic circuit without the need of additional electronic components. For instance, momentary switches will respond to one user-defined polarity of the magnetic field. However, latching switches will enable the realization of magnetic ON/OFF interfaces, which are not sensitive to the magnetic noise stemming from the surroundings. The reliable operation of magnetosensitive smart skins in complex environments with magnetic disturbances remains one of the key hurdles of current technologies for flexible magnetoelectronics.

We devise magnetosensitive smart skins with SV switches by attaching them to a pointing finger (Figure 3a). The device is connected in a 4-point configuration for the measurement of electrical resistance as it hovers over an interactive surface with magnetic stimuli. The surface contains two magnetic

buttons indicated as “ON” and “OFF”, which are represented by a permanent magnet with its South and North pole facing up, respectively (Figure 3b). These buttons can be used to switch on and off a virtual display showing a navigation route in a touchless way by approaching a finger with an on-skin

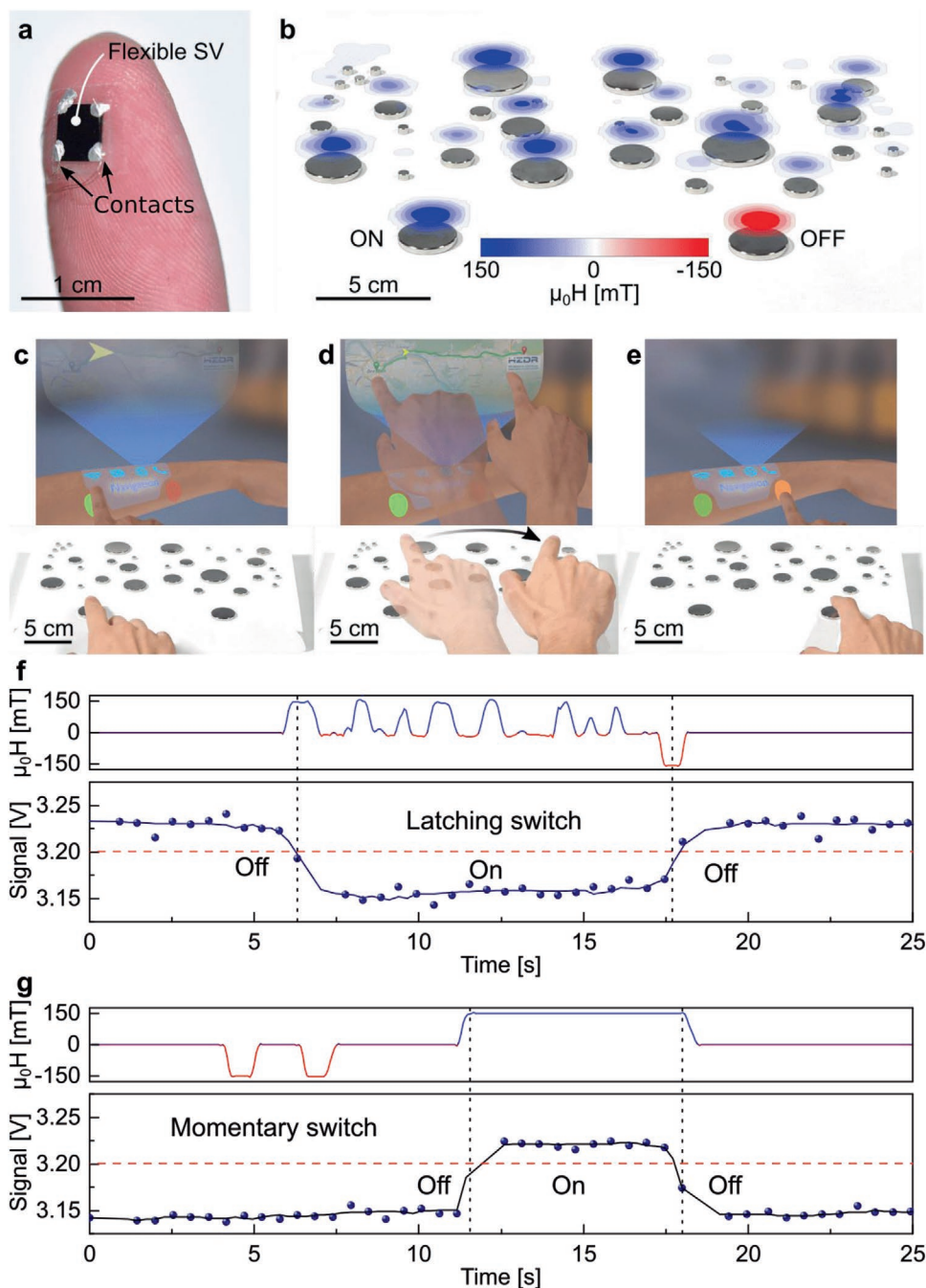


Figure 3. Momentary and latching switching capabilities. a) Flexible SV switch affixed on a pointing finger and contacted in a 4-point configuration. b) Array of magnets used in the demonstration. The color map represents the distribution of the out-of-plane component of the magnetic field measured 1 cm above the magnets surface. c–f) Latching switch performance of the SV with 3 nm thick Cu spacer. (c–e) Snapshots of the Movie S2, Supporting Information, showing the interactive process by switching ON and OFF the navigation software on a virtual display. f) Top panel represents the temporal variation of the magnetic field, which is experienced by the SV switch upon its motion above the array of magnets. Bottom panel shows the corresponding voltage readout. g) Momentary switching performance of the SV with 2 nm thick Cu spacer. Timeline of the magnetic field applied to the SV (top panel) and corresponding signal readout (bottom panel). The corresponding video sequence is shown in Movie S4, Supporting Information.

magnetosensitive element. To mimic magnetic disturbances, we assembled an array of permanent magnets of different sizes and strength as shown in Figure 3b. The contour plot over each magnet represents the spatial profile of the magnetic stray field 1 cm above the surface of the magnets (Figure S11, Supporting Information).

We note that the use of any magnetic field sensor including regular GMR multilayers enables the possibility to switch on and off the display (Movie S1 and Figure S12, Supporting Information). However, without additional electronic logic to condition the sensor, proximity sensors fail to operate in the presence of magnetic disturbances. Thus, after switching on the display upon approaching the GMR multilayer sensor to the ON button, the process of moving the finger above the array of permanent magnets leads to intermittent on-off switching of the virtual display.

In stark contrast, when using latching switches prepared based on the SV with a Cu spacer thickness of 3 nm, the device reveals a stable performance and is not affected by magnetic disturbances (Figure 3c–f and Movies S2 and S3, Supporting Information). In this case, the magnetoreceptor can be used to permanently switch the virtual display on upon approaching the magnetic ON button. The switching between ON and OFF states is recognized by crossing a pre-defined threshold of 3.2 V. The signal remains constant even as the SV is removed from the magnetic ON button and moved above the array of magnets. Accordingly, the virtual display stays ON independent of magnetic disturbances. To switch off the navigation panel, the magnetic OFF button is approached with the SV switch, which returns the signal to its initial value. In this example, the discrimination of the signal level and rejection of magnetic noise is done without any additional electronic components, just by using a flexible SV switch operating in the latching mode.

Another appealing functionality is offered by the momentary switch. This device is realized using a SV switch with a 2 nm thick Cu spacer layer. We program the SV device to respond to the positive magnetic field (corresponding to the ON button). These devices can be used to temporarily switch the virtual display on by approaching to the ON button but elicit no response when nearing the OFF button (Figure 3g and Movie S4, Supporting Information). This is a major advantage compared to the regular GMR multilayers, which possess a symmetric response curve and would equally be activated by magnetic fields of any polarity. Momentary switches can help to save energy by switching on the display only during the time when the SV is in the proximity to the ON button. The display goes off as soon as the finger is displaced away from the ON button.

3. Conclusions

In this work, we demonstrate the first flexible magnetoresistive spin valve switch operating with out-of-plane magnetic fields. By tailoring the magnetic exchange coupling in the complex layer stack, we realize SVs operating as latching (or permanent) switches and momentary switches. In this case, the magnetoresistive functional elements can perform basic logic operations (permanent or temporary switches) using a single material science platform. The enabled out-of-plane magnetic

field sensitivity of our flexible SVs makes the decision process upon interaction with magnetic objects obvious and unambiguous. To achieve stable mechanical performance of our SV devices, we rely on all-metallic layer stack based on Co/Pd multilayers with out-of-plane easy axis of magnetization. Furthermore, to avoid using antiferromagnets due to their brittleness, we utilize high performance synthetic antiferromagnets fabricated on flexible polymeric foils. Our SV devices prepared on 125 μm thick PEN foils withstand bending to 3.5 mm as well as repetitive bending tests over more than 600 cycles without sacrificing their magnetoresistive performance.

This technology expands the functionality of magnetoreceptive e-skins beyond basic proximity and orientation sensing. By tailoring the strength of the exchange bias between the sensing and reference layers of the spin valve, we were able to embed momentary and latching operation modes, thus reducing the complexity of external logic circuits. Unambiguous interpretation of the out-of-plane magnetic field provides intuitive on-off logic states and simplifies the use of the device. This new kind of flexible magnetoreceptive functional elements shows great potential for use in human-machine interfaces or virtual- and augmented reality applications. We showcase the advantages of this technology for the realization of on-skin interactive magnetoelectronics, which are touchless, energy efficient (momentary switches) and insensitive to external magnetic disturbances (latching switches).

4. Experimental Section

Fabrication: Spin valve switches consist of [Pd(0.9)/Co(0.4)]₄/Ru(0.4)/[Co(0.4)/Pd(0.9)]₃/Co(0.4)/Cu/[Co(0.4)/Pd(0.9)]₂ stacks (in brackets, the thicknesses of individual layers is indicated in nanometers). The thickness of the Cu spacer layer was varied from 2 to 5 nm. The samples were deposited at room temperature by DC magnetron sputtering (BESTEC, Germany) on 125 μm thick polyethylene naphthalate (PEN) polymeric foils purchased from Teijin corporation (Teonex). The surface roughness of the PEN foils was <0.7 nm. In line with the findings on CoFeB/Pt-based SAFs,^[47] a Ta(10 nm) / Pd(2.1 nm) seed layer was used to favor the growth of [Co/Pd] multilayers with [111] texture. The thickness of the individual layers and the number of repetitions in the [Co/Pd] stack were selected to ensure i) perpendicular magnetic anisotropy; ii) strong and compensated antiferromagnetic coupling in the SAF structure; and iii) two stable parallel/antiparallel magnetization configurations in the spin valve layer stack.^[48] A capping layer of Pd (2.1 nm) was deposited to prevent the magnetic free layer from oxidation. All the layers were deposited under an Ar pressure of 3.5×10^{-3} mbar while the deposition rate was set to 0.067 nm s⁻¹ (24 W) for Au, 0.03 nm s⁻¹ (40 W) for Ta, 0.04 nm s⁻¹ (26 W) for Pd, 0.025 nm s⁻¹ (52 W) for Co, and 0.03 nm s⁻¹ (48 W) for Ru. The magnetic and magnetoresistive performance of the samples are shown in Figures S3 and S4, Supporting Information. The observed change of the magnetic and magneto-resistive properties between the samples prepared on rigid and flexible support might be ascribed to a slightly higher average surface roughness of Teonex tapes (≈ 0.7 nm according to the data sheet) with respect to SiO_x/Si(100) rigid substrates (0.2–0.3 nm). The higher surface roughness could lead to surface inhomogeneity extending over the whole structure deposited on top, which might affect the PMA of the Co/Pd multilayers,^[49] the individual layer reversal,^[50] the interlayer exchange coupling in the synthetic antiferromagnetic reference layer,^[51] and the magnetoresistive properties of the whole GMR spin-valve stack.^[52] In particular, the increased interface roughness might explain the reduction of the GMR ratio as well as the changes of the MR curves for $t_{\text{Cu}} = 2$ nm, which could originate from an interlayer coupling between the free layer and the top

SAF layer induced by interlayer magnetostatic interactions (orange-peel Néel coupling) or a direct exchange coupling through the formation of pinholes in the Cu spacer layer.

GMR multilayers consist of $[\text{Co}(1 \text{ nm})/\text{Cu}(2.2 \text{ nm})]_{50}$ stacks coupled at the 2nd antiferromagnetic maximum. The layer stack was deposited on a polyester foil (Melinex ST505) with a thickness of $175 \mu\text{m}$ by DC magnetron sputtering at room temperature (Ar was used as a sputter gas; Ar pressure was 8×10^{-4} mbar; base pressure was 10^{-7} mbar; deposition rate was 0.2 nm s^{-1}). The magnetoresistive curve of the samples is shown in Figure S9, Supporting Information.

Transparency Measurements: Due to the difference in the thickness of the layer stack, the SV switches and GMR multilayers revealed a different level of transparency (Figure S2, Supporting Information). In these measurements, a reflective neutral density optical filter (Thorlabs, USA) was placed between an HXP 120 V (Zeiss, Germany) light source and the sample, to reduce the intensity of the source. The incoming light was transmitted through the sample, collected and analyzed with a USB 650 spectrometer (Ocean Insight, USA). Two segments of the optical fiber were placed before and after the sample to guide and gathered the incoming and transmitted light, respectively.

Electron Microscopy: TEM analysis was performed by means of a Philips CM200 microscope on cross sectioned films. TEM samples were prepared relying on a thinning procedure consisting of mechanical thinning by grinding papers, diamond pastes, and a dimple grinder. Final thinning was carried out with a precision ion polishing system (GATAN 691). SEM images were obtained using a Phenom XL Desktop Scanning Electron Microscope. For imaging of the samples in a bent state, the SV was fixed in a tensile tester sample holder and bent to the desired radius of curvature.

Integral Magnetic Properties: Magnetic hysteresis loops were investigated at room temperature by using a vibrating sample magnetometer (Model 10, MicroSense) equipped with a rotating electromagnet that could supply a maximum field of 2 T.

Magnetoresistive Responses: Magnetoresistive performance of the SVs in the bent state was investigated by applying an out-of-plane magnetic field with an electromagnet powered by bipolar power supply (Kepco, USA). A maximum field of 500 mT (150 mT) was applied for full (minor) loop measurements. The resistance of the SVs was monitored in a 4-wire configuration using a tensorometer setup (HZDR Innovation GmbH, Germany). Room temperature magneto-transport properties were measured on square-shaped samples employing the van der Pauw method in current-in-plane geometry. Currents in the order of 10 mA were injected using a Keithley 6221 current source, while voltages were measured by a Keithley 2182A nanovoltmeter. The magnetic field was provided by a dipole electromagnet (GMW Associates, USA).

Bending Performance: Static mechanical bending tests were performed using a custom built bending setup. SV switches were horizontally fixed using two clamps and bent to the desired curvature radius by gradual decrease of the distance between the clamps. The change of the bending radius along the sample was determined from the analysis of the optical photographs of the bent sample (Figure S7, Supporting Information). Magnetoresistive performance was measured in bent and flattened states. The characterization of the SV under dynamic bending conditions was performed using a Tensile Sample Holder of the Phenom XL SEM. The SV was mounted in the same manner as for static bending experiments. The sample holder was programmed to repeatedly bend the SV between 28 and 14 mm bending radii. A 4-wire resistance of the SV was continuously monitored using a digital multimeter (Keysight 34461A; Keysight Technologies, USA).

Interactive Magnetoreceptor Demonstrators: A flexible SV switch with a lateral dimension of $4 \times 4 \text{ mm}^2$ was fixed on a pointing finger and electrically connected in a four-point configuration using $50 \mu\text{m}$ thick copper wires with a conductive silver paste. To mimic spatially varying magnetic disturbances, an array of NdFeB magnets of different dimensions was assembled (HKCM Engineering e.K., Germany). All magnets in the array were oriented with their South pole facing up. Two magnets (indicated in Figure 3 with “On”/“Off”) represent interactive magnetic buttons to start/stop a navigation software. These

two magnets were oriented in the following way: “On” magnet with its south pole facing up and “Off” magnet with its north pole facing up.

For the measurement of the sensor response, the current to the SV was supplied by a Source/Measure unit (B2902A, Keysight Technologies, USA) and the voltage was first pre-amplified and then readout by a DAQ (National Instruments, USB-6009, USA). The sensor response was analyzed by a NI LabVIEW (2019 SP1 version) script, which was controlling the frames of the representative animation. Crossing the pre-defined voltage threshold of 3.2 V was recognized as either an “On” or “Off” command. Prior to the demonstration both of the switches were programmed to respond to positive magnetic field by subjecting them to -450 mT using a permanent magnet.

Mapping the Magnetic Stray Fields: The magnetic stray field produced by the array of magnets in Figure 3 (see also Figure S10, Supporting Information) was measured with a Gaussmeter (HGM09s, MAGSYS, Germany) mounted on a micromanipulator. The Hall probe of the Gaussmeter was swept in the plane parallel to the plane of the magnets at a distance of 1 cm. In this measurement, only the out-of-plane component of the magnetic stray field was detected.

Strain Calculation: The strain distribution along the SV upon bending was estimated using the following equation:^[53]

$$\varepsilon = \frac{(d_f + d_s)}{2R} \frac{(1 + 2\eta + \chi\eta^2)}{(1 + \eta)(1 + \chi\eta)} \quad (1)$$

where $\eta = d_{sv} / d_s$ and $\chi = Y_{sv} / Y_s$. d_{sv} is the total thickness of the spin valve metal stack and d_s is the substrate thickness (125- μm -thick PEN). The Young's modulus of the metallic film (Y_{sv}) was calculated to be 180 GPa, assuming a composite structure of the stack and taking into account the mechanical properties of the corresponding bulk metals (177 GPa for Pd, 211 GPa for Co, 414 GPa for Ru, 110 GPa for Cu, and 186 GPa for Ta). The Young's modulus of the PEN substrate (Y_s) was taken as 2.2 GPa. ε is the surface strain in metal layers when the structure is bent to a radius R .

Use of On-Skin Electronics: The measurements using on-skin electronics were performed with the consent of all volunteers who participated in the study.

Supporting Information

Supporting Information is available from the Wiley Online Library or from the author.

Acknowledgements

The authors thank Dr. Minjeong Ha (HZDR) for her support at the initial stages of the project. Support by the Structural Characterization Facilities Rossendorf at the Ion Beam Center (IBC) at the HZDR is greatly appreciated. This work was financed in part via the German Research Foundation (DFG) grants MA 5144/9-1 and MA 5144/13-1, MA 5144/28-1 and Helmholtz Association of German Research Centres in the frame of the Helmholtz Innovation Lab “FlexiSens”. C.R. acknowledges the PRIN project TWEET by MIUR (No. 2017YCTB59).

Open access funding enabled and organized by Projekt DEAL.

Conflict of Interest

The authors declare no conflict of interest.

Data Availability Statement

The data that support the findings of this study are available from the corresponding author upon reasonable request.

Keywords

flexible electronics, flexible spin valve, magnetic field sensors, sensors, skin-conformal

Received: February 1, 2021

Revised: March 4, 2021

Published online: March 26, 2021

- [1] Y. Liu, S. Mo, S. Shang, P. Wang, W. Zhao, L. Li, *J. Sci.: Adv. Mater. Devices* **2020**, 5, 451.
- [2] W. Gao, H. Ota, D. Kiriya, K. Takei, A. Javey, *Acc. Chem. Res.* **2019**, 52, 523.
- [3] J. A. Rogers, T. Someya, Y. Huang, *Science* **2010**, 327, 1603.
- [4] Q. Hua, J. Sun, H. Liu, R. Bao, R. Yu, J. Zhai, C. Pan, Z. L. Wang, *Nat. Commun.* **2018**, 9, 244.
- [5] M. Kaltenbrunner, T. Sekitani, J. Reeder, T. Yokota, K. Kuribara, T. Tokuhara, M. Drack, R. Schwödiauer, I. Graz, S. Bauer-Gogonea, S. Bauer, T. Someya, *Nature* **2013**, 499, 458.
- [6] Y. Wan, Y. Wang, C. F. Guo, *Mater. Today Phys.* **2017**, 1, 61.
- [7] J. Zhao, H. Guo, Y. K. Pang, F. Xi, Z. W. Yang, G. Liu, T. Guo, G. Dong, C. Zhang, Z. L. Wang, *ACS Nano* **2017**, 11, 11566.
- [8] Z. Wang, T. Wang, M. Zhuang, H. S. Xu, *ACS Appl. Mater. Interfaces* **2019**, 11, 45301.
- [9] J.-H. Seo, E. Swinnich, Y.-Y. Zhang, M. Kim, *Mater. Res. Lett.* **2020**, 8, 123.
- [10] B. Zhang, Z. Xiang, S. Zhu, Q. Hu, Y. Cao, J. Zhong, Q. Zhong, B. Wang, Y. Fang, B. Hu, J. Zhou, Z. Wang, *Nano Res.* **2014**, 7, 1488.
- [11] M. S. Sarwar, Y. Dobashi, C. Preston, J. K. M. Wyss, S. Mirabbasi, J. D. W. Madden, *Sci. Adv.* **2017**, 3, e1602200.
- [12] J. Ge, L. Sun, F.-R. Zhang, Y. Zhang, L.-A. Shi, H.-Y. Zhao, H.-W. Zhu, H.-L. Jiang, S.-H. Yu, *Adv. Mater.* **2015**, 28, 722.
- [13] M. Melzer, M. Kaltenbrunner, D. Makarov, D. Karnaushenko, D. Karnaushenko, T. Sekitani, T. Someya, O. G. Schmidt, *Nat. Commun.* **2015**, 6, 6080.
- [14] D. Makarov, M. Melzer, D. Karnaushenko, O. G. Schmidt, *Appl. Phys. Rev.* **2016**, 3, 11101.
- [15] G. S. C. Bermúdez, D. D. Karnaushenko, D. Karnaushenko, A. Lebanov, L. Bischoff, M. Kaltenbrunner, J. Fassbender, O. G. Schmidt, D. Makarov, *Sci. Adv.* **2018**, 4, eaao2623.
- [16] M. Kondo, M. Melzer, D. Karnaushenko, T. Uemura, S. Yoshimoto, M. Akiyama, Y. Noda, T. Araki, O. G. Schmidt, T. Sekitani, *Sci. Adv.* **2020**, 6, eaay6094.
- [17] G. S. C. Bermúdez, H. Fuchs, L. Bischoff, J. Fassbender, D. Makarov, *Nat. Electron.* **2018**, 1, 589.
- [18] J. Ge, X. Wang, M. Drack, O. Volkov, M. Liang, G. S. C. Bermúdez, R. Illing, C. Wang, S. Zhou, J. Fassbender, M. Kaltenbrunner, D. Makarov, *Nat. Commun.* **2019**, 10, 4405.
- [19] Z. Wang, X. Wang, M. Li, Y. Gao, Z. Hu, T. Nan, X. Liang, H. Chen, J. Yang, S. Cash, N.-X. Sun, *Adv. Mater.* **2016**, 28, 9370.
- [20] N. Pérez, M. Melzer, D. Makarov, O. Uebberschär, R. Ecke, S. E. Schulz, O. G. Schmidt, *Appl. Phys. Lett.* **2015**, 106, 153501.
- [21] S. Ota, M. Ono, H. Matsumoto, A. Ando, T. Sekitani, R. Kohno, S. Iguchi, T. Koyama, D. Chiba, *Appl. Phys. Express* **2019**, 12, 053001.
- [22] G. V. Kurylanskaya, E. Fernández, A. Svalov, A. B. Beitia, A. García-Arribas, A. Larrañaga, *J. Magn. Magn. Mater.* **2016**, 415, 91.
- [23] S. S. P. Parkin, K. P. Roche, T. Suzuki, *Jpn. J. Appl. Phys.* **1992**, 31, L1246.
- [24] F. Yan, G. Xue, F. Wan, *J. Mater. Chem.* **2002**, 12, 2606.
- [25] T. Uhrmann, L. Bär, T. Dimopoulos, N. Wiese, M. Rührig, A. Lechner, *J. Magn. Magn. Mater.* **2006**, 307, 209.
- [26] Y.-f. Chen, Y. Mei, R. Kaltofen, J. I. Mönch, J. Schumann, J. Freudenberger, H.-J. Klauß, O. G. Schmidt, *Adv. Mater.* **2008**, 20, 3224.
- [27] B. Özkaya, S. R. Saranu, S. Mohanan, U. Herr, *Phys. Status Solidi (a)* **2008**, 205, 1876.
- [28] C. Barraud, C. Deranlot, P. Seneor, R. Mattana, B. Dlubak, S. Fusil, K. Bouzehouane, D. Deneuve, F. Petroff, A. Fert, *Appl. Phys. Lett.* **2010**, 96, 072502.
- [29] a) A. Bedoya-Pinto, M. Donolato, M. Gobbi, L. E. Hueso, P. Vavassori, *Appl. Phys. Lett.* **2014**, 104, 062412; b) A. Bedoya-Pinto, M. Donolato, M. Gobbi, L. E. Hueso, P. Vavassori, *Appl. Phys. Lett.* **2014**, 104, 119902.
- [30] T. Griesbach, M. C. Wurz, L. Rissing, *IEEE Trans. Magn.* **2012**, 48, 3843.
- [31] A. Alfadhel, J. Kosel, *Adv. Mater.* **2015**, 27, 7888.
- [32] B. Li, M. N. Kavaldzhiev, J. Kosel, *J. Magn. Magn. Mater.* **2015**, 378, 499.
- [33] H. Li, Q. Zhan, Y. Liu, L. Liu, H. Yang, Z. Zuo, T. Shang, B. Wang, R.-W. Li, *ACS Nano* **2016**, 10, 4403.
- [34] M. Melzer, D. Makarov, O. G. Schmidt, *J. Phys. D: Appl. Phys.* **2019**, 53, 083002.
- [35] P. N. Granell, G. Wang, G. S. C. Bermúdez, T. Kosub, F. Golmar, L. Steren, J. Fassbender, D. Makarov, *npj Flexible Electron.* **2019**, 3, 3.
- [36] M. Melzer, J. I. Mönch, D. Makarov, Y. Zabala, G. S. C. Bermúdez, D. Karnaushenko, S. Baunack, F. Bahr, C. Yan, M. Kaltenbrunner, O. G. Schmidt, *Adv. Mater.* **2014**, 27, 1274.
- [37] Z. Wang, M. Shaygan, M. Otto, D. Schall, D. Neumaier, *Nanoscale* **2016**, 8, 7683.
- [38] H. Heidari, E. Bonizzoni, U. Gatti, F. Maloberti, R. Dahiya, *IEEE Sens. J.* **2016**, 16, 8736.
- [39] I. J. Monch, F. Bahr, M. Melzer, D. Karnaushenko, D. Makarov, W. Hofmann, O. G. Schmidt, *IEEE Trans. Magn.* **2015**, 51, 1.
- [40] G. A. Salvatore, N. Münzenrieder, T. Kinkeldei, L. Petti, C. Zysset, I. Strebel, L. Bütke, G. Tröster, *Nat. Commun.* **2014**, 5, 2982.
- [41] L. Petti, N. Münzenrieder, C. Vogt, H. Faber, L. Bütke, G. Cantarella, F. Bottacchi, T. D. Anthopoulos, G. Tröster, *Appl. Phys. Rev.* **2016**, 3, 021303.
- [42] G. Varvaro, *Ultrahigh-Density Magnetic Recording: Storage Materials and Media Designs*, Pan Stanford Publishing CRC Press, Taylor & Francis Group, London **2016**.
- [43] S. S. P. Parkin, *Appl. Phys. Lett.* **1996**, 69, 3092.
- [44] M. Melzer, G. Lin, D. Makarov, O. G. Schmidt, *Adv. Mater.* **2012**, 24, 6468.
- [45] W. Cheng, Z. Zhou, M. Pan, H. Yang, Y. Xie, B. Wang, Q. Zhan, R.-W. Li, *J. Phys. D: Appl. Phys.* **2018**, 52, 095003.
- [46] H. Ehrenreich, *Solid State Physics: Advances in Research and Applications*, Academic Press, London **2001**.
- [47] T. Vermulker, R. Mansell, A. Fernández-Pacheco, R. P. Cowburn, *Adv. Funct. Mater.* **2016**, 26, 4704.
- [48] G. Varvaro, S. Laureti, D. Peddis, M. Hassan, G. Barucca, P. Mengucci, A. Gerardino, E. Giovine, O. Lik, D. Nissen, M. Albrecht, *Nanoscale* **2019**, 11, 21891.
- [49] J. Qiu, Z. Meng, Y. Yang, J. F. Ying, Q. J. Yap, G. Han, *AIP Adv.* **2016**, 6, 056123.
- [50] S. Nakagawa, H. Yoshikawa, *J. Magn. Magn. Mater.* **2005**, 287, 193.
- [51] M. Desai, A. Misra, W. D. Doyle, *IEEE Trans. Magn.* **2005**, 41, 3151.
- [52] E. Y. Tsybal, D. G. Pettifor, *Solid State Phys.* **2001**, 56, 113.
- [53] Z. Suo, E. Y. Ma, H. Gleskova, S. Wagner, *Appl. Phys. Lett.* **1999**, 74, 1177.